

Singlet–Triplet and Triplet–Triplet Interactions in Conjugated Polymer Single Molecules

Ji Yu, Robin Lammi, Andre J. Gesquiere, and Paul F. Barbara*

Center for Nano- and Molecular Science and Technology and Department of Chemistry and Biochemistry, University of Texas at Austin, Austin, Texas 78712

Received: February 7, 2005; In Final Form: March 25, 2005

Single molecule fluorescence correlation spectroscopy has been used to investigate the photodynamics of isolated single multichromophoric polymer chains of the conjugated polymers MEH-PPV and F8BT on the microsecond to millisecond time scale. The experimental results (and associated kinetic modeling) demonstrate that (i) triplet exciton pairs undergo efficient triplet–triplet annihilation on the $\ll 30 \mu\text{s}$ time scale, (ii) triplet–triplet annihilation is the dominant mechanism for triplet decay at incident excitation powers $\geq 50 \text{ W/cm}^2$, and (iii) singlet excitons are quenched by triplet excitons with an efficiency on the order of $1/2$. The high efficiency of this latter process ensures that single molecule fluorescence spectroscopy can be effectively used to indirectly monitor triplet exciton population dynamics in conjugated polymers. Finally, correlation spectroscopy of MEH-PPV molecules in a multilayer device environment reveals that triplet excitons are efficiently quenched by hole polarons.

I. Introduction

Singlet–triplet exciton interactions in conjugated polymers may play a significant role in electroluminescent organic light emitting displays (OLED) and other optoelectronic devices. While singlet and triplet excitons are both simultaneously present in an OLED due to electron–polaron/hole–polaron recombination, triplet excitons are nonradiative and do not contribute to the electroluminescence. Due to the faster rate of formation of triplets and the fact that triplets have a substantially longer lifetime than singlet excitons, triplets are present in much higher average concentration in a device.^{1,2} Triplet excitons can in principle indirectly influence the electroluminescence intensity for an OLED as a result of singlet exciton “quenching” by triplets via a charge transfer or/and energy transfer mechanism.^{3–6} Thus, a thorough and quantitative understanding of singlet–triplet interactions is critical to the development of predictive models for device function.

Unfortunately, it is exceedingly difficult to unravel the complex and heterogeneous kinetics of a functioning conjugated polymer device due to three factors: (i) the large number of different excitonic and polaronic species in the device, (ii) the potential for large spatial variations and fluctuations in the concentration of these species, and (iii) the large *morphological heterogeneity* of the conjugated polymer material itself. These complications can be partially avoided by time-resolved photoinduced absorption and photoinduced emission studies which offer more control over the populations of specific exciton and/or polarons.^{7–15}

An alternative approach that has been used to investigate the spectroscopy of conjugated polymers is single molecule spectroscopy (SMS) of isolated polymer chains. This is typically achieved at high dilution in an inert polymer host using ultrapure sample preparation methods.¹⁶ There are several advantages of the SMS approach.^{6,17–33} By investigating one molecule at a time this technique can greatly minimize spectral and kinetic

heterogeneity. This in turn allows for both the unraveling of complex kinetic mechanisms and the determination of distribution functions for rate constants, not just ensemble average values. In particular, each isolated chain in the SMS approach is large enough (typically 10^4 – 10^6 amu)^{34–45} to be representative of the bulk in terms of spectroscopic properties and the presence of multiple chromophoric sites, but small enough to be “morphologically simple” (typically involving at most one morphological feature, e.g., chain–chain contact).³⁷ Furthermore, by employing isolated polymer chains rather than bulk materials the diffusion of excitons and polarons is confined to a single particle and to a short separation distance.

This paper reports the first SMS study of conjugated polymers on the submillisecond to microseconds time scale.^{34–52} Two intramolecular processes, triplet–triplet annihilation and singlet quenching by triplets, are investigated in detail for the investigated polymer materials: poly[2-methoxy-5-(2'-ethylhexyloxy)-*p*-phenylene vinylene] (MEH-PPV) and poly(9,9'-diocetylfluorene-cobenzothiadiazole) (F8BT), see Figure 1. The experimental results, which have been acquired with continuous wave (cw) excitation and analyzed by fluorescence intensity autocorrelation, offer new insights on triplet–triplet and singlet–triplet interactions in conjugated polymers. In addition, the interaction of triplet excitons with hole polarons is investigated for MEH-PPV in a device environment demonstrating that at high hole concentration, charge-transfer-induced quenching rather than triplet annihilation becomes the dominant mechanism for triplet decay in this conjugated polymer under high excitation conditions.

II. Experimental Section

Individual F8BT or 1,1'-didodecyl-3,3,3',3'-tetramethylindocarbocyanine perchlorate (DiI) molecules were isolated in an inert polystyrene (PS) film by spin coating a F8BT/PS solution on to a microscope glass coverslip. For MEH-PPV poly(methyl methacrylate) (PMMA) was used as the polymer host. The resulting film thicknesses for PS and PMMA were ~ 200 and 100 nm , respectively. Samples were overcoated with 200 nm

* To whom correspondence should be addressed. E-mail: p.barbara@mail.utexas.edu.

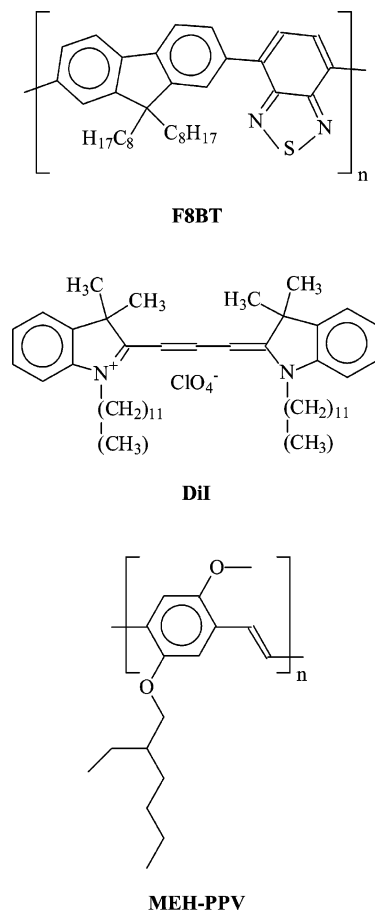


Figure 1. Chemical structures for the multichromophoric conjugated polymers F8BT and MEH-PPV, and the single chromophore dye DiI.

of aluminum or gold in a vacuum in order to reduce the concentration of O_2 molecules in the films, which quench the triplet excitons and induce photochemistry. No metal overlayer was employed for the DiI samples. Single molecule fluorescence images and transient data were recorded with a home-built sample scanning confocal fluorescence microscope, which has been described elsewhere.¹⁶ Single molecules were positioned at the center of the focused excitation laser beam (514 nm for MEH-PPV, 488 nm for DiI, and 457 nm for F8BT). The fluorescence was detected by an avalanche photodiode (APD) (Perkin-Elmer Optoelectronics SPCM-AQR-15). The intensity autocorrelation data were acquired with an ALV5000/E real time autocorrelator with one APD (for autocorrelation) or alternatively two APD detectors (for pseudo-cross-correlation). The APDs were chosen carefully from a set of alternative devices to minimize artifacts in the signal due to after-pulsing. Observed autocorrelation dynamics and amplitudes were confirmed for representative conditions by pseudo-cross-correlation with two detectors, which is a method that is less susceptible to artifacts due to after-pulsing.

III. Basic Observations and Techniques

A. Background. Previous SMS studies on conjugated polymers have shown that singlet excitons are efficiently “funneled” by energy transfer to a small number of sites in a single isolated conjugated polymer molecule chain, resulting in red-shifted emission spectra and site-localized photochemistry and photophysics.^{36,37} This surprisingly efficient and directional energy transport (energy funneling) is attributed to a highly ordered conformational structure resulting from conjugated

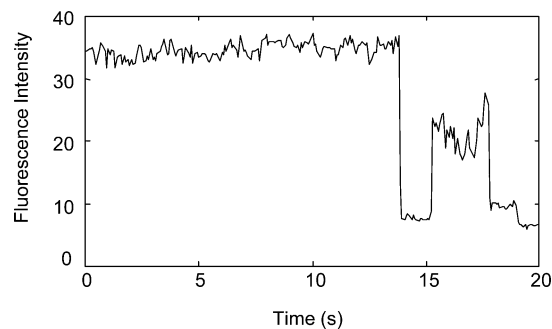


Figure 2. Fluorescence transient of a single F8BT molecule from a sample sealed with aluminum, showing single step blinking of the fluorescence intensity.

polymer-chain folding. It is well established that an individual conjugated polymer single molecule behaves as a multichromophoric molecular system due to a distribution of conjugated segments on the polymer chain connected by chemical and structural defects. For the MEH-PPV molecules in this study ($MW \sim 10^6$), there are ~ 200 effective chromophores, each with ~ 10 – 17 repeat units in conjugation length, in a single molecule. Absorption of photons excites different chromophores on the polymer chain. A “folded” single MEH-PPV molecule is approximately 10 nm in radius. For the F8BT molecules in this study ($MW \sim 10^5$), there are ~ 50 effective chromophores, each with ~ 4 – 5 repeat units in conjugation length, in a single molecule with an approximate radius of 5 nm. DiI^{53–56} is included in this study as a “single chromophore” reference material that is *incapable of exhibiting binary or higher exciton interactions in isolated single molecules*.

B. Slow Fluorescence Dynamics. Figure 2 shows a typical fluorescence time transient for the conjugated polymer F8BT irradiated by a cw excitation in resonance with the lowest energy absorption band. Similar results are observed for MEH-PPV.^{36,57} At long time scales discrete reversible “drops” in the intensity are observed due to photooxidation (typically several minutes after the irradiation is initiated, and only in the presence of oxygen impurities). At the exact time of photooxidation the overall fluorescence intensity is observed to decrease due to efficient quenching by an excess positive charge, i.e., hole-polaron, which is photoinjected by the oxidation process.

Here we describe a detailed investigation of the fluorescence intensity dynamics *before photobleaching*. We analyze and assign previously unreported intensity fluctuations, due to short-lived triplet excitons that cause significant quenching of singlet excitons. Since the time scale for these fluctuations is < 1 ms direct intensity vs time studies are not possible due to a poor signal-to-noise ratio from shot noise for short “dwell times”. Instead, we have used fluorescence intensity autocorrelation analysis, which determines the statistical properties of the stochastic temporal fluctuations for a steady-state photodynamic system under constant irradiation conditions. This technique has been used to study a variety of photophysical processes including the population/depopulation of long-lived triplet states in dye molecules.^{16,56,58–64} Typically, fluorescence intensity fluctuations are analyzed via the second-order intensity autocorrelation function,^{16,62}

$$G(\tau) = \frac{\langle F(t)F(t+\tau) \rangle}{\langle F \rangle^2} - 1 \quad (1)$$

where $F(t)$ is the fluorescent intensity at time t and the broken brackets represent time average. $G(\tau)$ data for DiI and the conjugated polymers are shown in Figure 3.

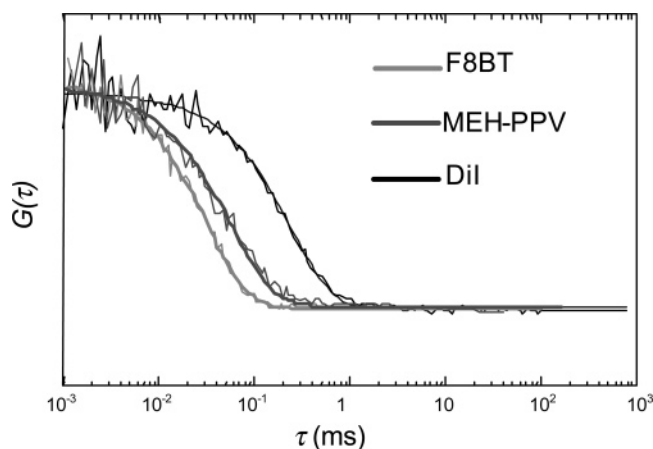


Figure 3. Experimental fluorescent intensity autocorrelation transients (best-fit by a single-exponential decay) for typical single molecules of (from left to right) F8BT, MEH-PPV, and DiI. The correlation function contrast was normalized for the shown $G(\tau)$ data. The F8BT samples were sealed with aluminum, the MEH-PPV sample was sealed with gold, and the DiI samples were unsealed.

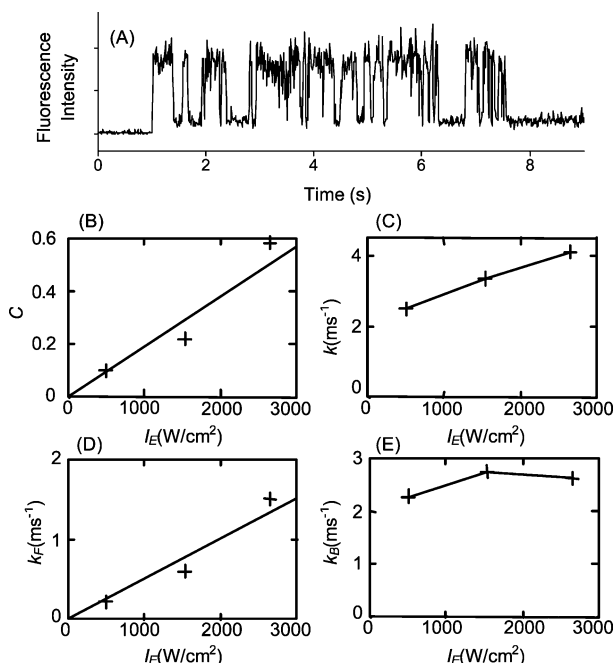


Figure 4. (A) Fluorescence trajectory of a single DiI molecule. Fast single-step on–off blinking of the fluorescence intensity is evident. Correlation function contrast C (B), relaxation decay rate k (C), and the calculated forward (D) and backward rate (E), obtained on the same DiI molecule, are plotted as a function of excitation intensity.

C. Single Chromophore Example. To build a framework for analyzing $G(\tau)$ data for multichromophoric molecules undergoing triplet population dynamics (such as conjugated polymers), it is useful to review the framework for analyzing $G(\tau)$ data of a single chromophoric dye molecule (DiI). For DiI the triplet state is *populated* through intersystem crossing (ISC) from the excited singlet state and *depopulated* through reverse intersystem crossing to the singlet ground state. $F(t)$ exhibits a telegraphic-like (fluorescence blinking) signal due to the intermittent formation of a long-lived triplet state (Figure 4A), which is highly consistent with a simple three-level photodynamic scheme including the ground and first excited singlet states (S_0 and S_1) and the triplet state T_1 .¹⁶ Under low to moderate irradiation intensities the three-level scheme can be further approximated by an even simpler two-state model,¹⁶



with opposing forward and backward first-order rate constants, k_F and k_B , that are given by,

$$k_F = k_{\text{exc}} k_{\text{isc}} \tau_{\text{fl}} \quad (3)$$

$$k_B = k'_{\text{isc}} \quad (4)$$

where k'_{isc} is the reverse ISC rate, k_{isc} is the ISC rate, and τ_{fl} is the fluorescence lifetime. The excitation rate k_{exc} is given by:

$$k_{\text{exc}} = \frac{I_E \sigma}{h\nu} \quad (5)$$

where I_E is the incident excitation intensity, σ is the absorption cross-section of the molecule, and $h\nu$ is the energy of the photons.

Importantly, this model predicts that $G(\tau)$ should be a single-exponential decay.

$$G(\tau) = C e^{-k\tau} \quad (6)$$

k_F and k_B can be determined experimentally from the “contrast” C and the “relaxation rate constant” k by using the following relationships,⁶⁵

$$k = k_B + k_F \quad (7)$$

$$C = \frac{k_F}{k_B} \quad (8)$$

Figure 4D–E shows estimates for k_F and k_B based on experimental C and k values for the same DiI molecule under three different excitation powers. The results show, as expected from eqs 1–8, a linear power dependence for k_F and no power dependence for k_B .^{66,67} Furthermore, as expected, the steady-state fluorescence intensity vs irradiation intensity exhibits saturation at high irradiation intensity (Figure 5) due to steady-state buildup of the triplet state. Indeed, the saturation effect is in quantitative agreement with predictions based on the k_F and k_B values from the correlation analysis, further supporting the validity of the simple two-state model.

D. Correlation Data for F8BT and MEH-PPV. It is interesting to compare and contrast the fluorescence intensity autocorrelation data for DiI with that for the multichromophoric molecules F8BT and MEH-PPV. Figure 3 compares typical autocorrelation curves for isolated F8BT, MEH-PPV, and DiI molecules. In analogy with DiI, the conjugated polymers show a large-amplitude autocorrelation signal suggesting blinking due to triplet formation and decay. As expected for intensity fluctuations due to triplet states, the autocorrelation traces are strongly dependent on the concentration of oxygen dissolved in the polymer matrix, as shown in Figure 6 for F8BT. The results in Figure 6A were obtained from a single polymer chain in a freshly prepared aluminum-coated sample (in order to exclude oxygen), with oxygen pressures as low as 6×10^{-7} Torr. Figure 6B shows a representative trace for a molecule in a sample exposed to ambient oxygen (~ 158 Torr), and Figure 6C depicts the autocorrelation obtained for the same molecule in an argon-rich environment. The average autocorrelation rate measured for molecules in the aluminum-coated sample is 108 ms^{-1} . For molecules studied in uncoated films under argon flow the decay rate is faster (221 ms^{-1}), which is not surprising considering the difficulty of excluding oxygen with an open

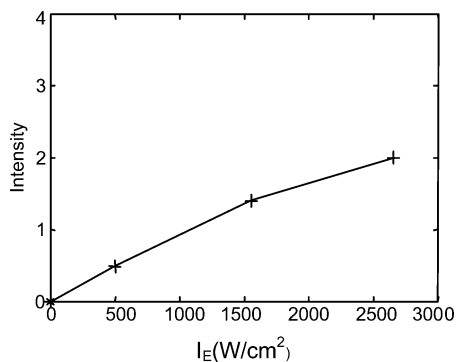


Figure 5. Plot of the measured DiI fluorescence intensity as a function of excitation intensity. The fluorescence intensity saturates at higher excitation intensities.

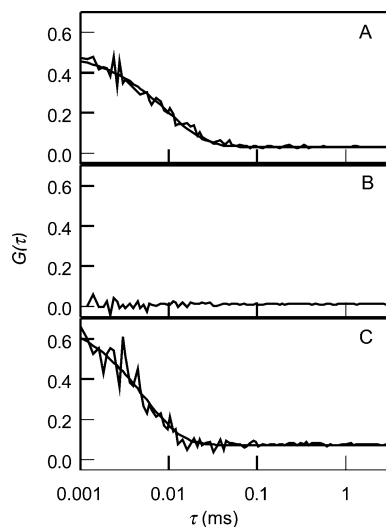


Figure 6. Intensity autocorrelation traces for isolated F8BT molecules in polystyrene films: (A) Film exposed to vacuum ($\sim 6 \times 10^{-7}$ Torr) and coated with aluminum (100 nm) prior to spectroscopic studies. Decay was fit to a single exponential with a rate of 103 ms^{-1} ($C = 0.47$). (B) A single molecule in a film exposed to ambient oxygen (~ 158 Torr). (C) The same single molecule as in part B after purging with Ar flow. Decay was fit to a single exponential with a rate of 189 ms^{-1} ($C = 0.64$).

flow system. Finally, the same polymers studied under ambient oxygen exhibit fluctuations that are too fast to resolve. These observations strongly suggest that isolated F8BT triplets are quenched by oxygen in the polystyrene matrix.

Despite the expectation of many accessible states and processes for F8BT and the potential for having more than one triplet exciton per molecule at the same time, experimental $G(\tau)$ data for F8BT (Figure 7A) are surprisingly simple. Autocorrelation curves for virtually all molecules that have been investigated in a large ensemble are well-fit by a single-exponential decay. While the contrast ratio (see Figure 7B) and correlation times vary from molecule to molecule and as a function of excitation intensity (Figure 8) for the same molecule, a single-exponential behavior is observed in all cases within experimental error. This suggests that an approximate two-state model should be suitable for F8BT. Analogously, single exponential $G(\tau)$ data for MEH-PPV (e.g. Figure 3) suggest that an approximate two-state model is also suitable for MEH-PPV.

IV. Multichromophoric Photodynamic Model

A. Basic Model. We now consider various simple kinetic models for the photodynamics of isolated multichromophoric

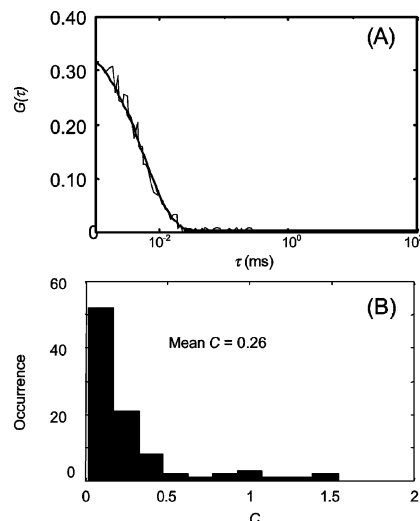


Figure 7. (A) Fluorescence intensity correlation for an individual F8BT molecule in a sample sealed with aluminum. The relaxation time is on the order of $10 \mu\text{s}$ as determined by fitting to eq 6 (solid line). (B) A histogram of the autocorrelation function contrast for many F8BT molecules is shown. A broad distribution of the autocorrelation contrast can be observed, with an average contrast of 0.26.

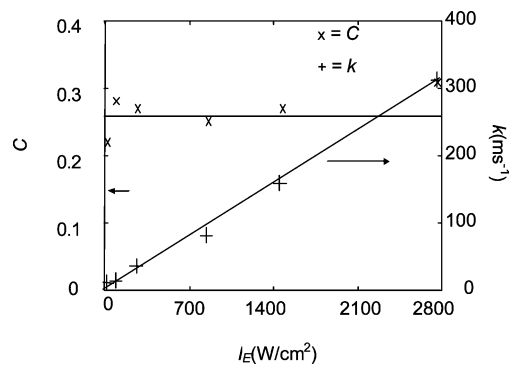
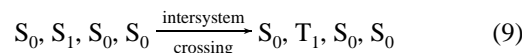
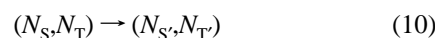


Figure 8. The autocorrelation contrast C and relaxation decay rate k plotted versus excitation intensity for a single F8BT molecule in a sample sealed with aluminum. The decay rate increases linearly with excitation intensity while the autocorrelation contrast saturates.

molecules. Our starting point assumes that the photodynamics are well described by a set of first-order incoherent rate processes connecting population states of the system that correspond to each localized chromophore occupying S_0 , S_1 , and T_1 at a given time. For a simple example, consider the intersystem crossing of a molecule comprised of four distinguishable weakly coupled chromophores with the second chromophore occupying S_1 and the other three occupying S_0 .



This scheme can be even further simplified by assuming that only the number of each type of excitations matters, not the specific configuration of these excitations in the polymer chain. This approximation would be valid for example if triplet exciton diffusion was sufficiently rapid to ensure “homogeneous” kinetics and there was a narrow distribution of site energies. Based on this simplification we can replace the configurations of eq 9 with even simpler population states, i.e.



where N_S and N_T are the number of singlet and triplet excitons

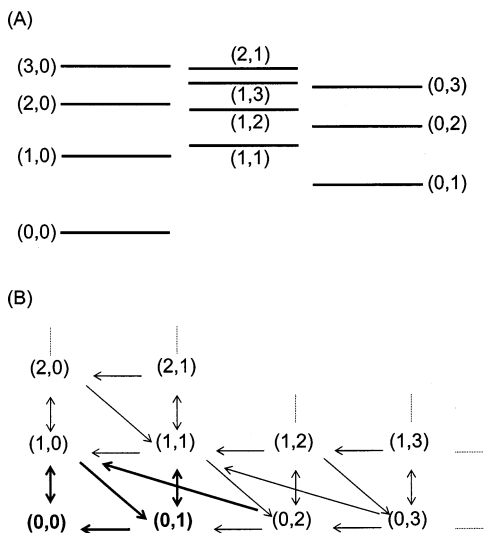


Figure 9. (A) Energy diagram and (B) kinetic scheme representing the processes at play in the population state model. For conjugated polymers this model can be reduced to the processes indicated with bold arrows.

before and after the specific relaxation process, and $N_S + N_T \leq N_C$, where N_C is the total number of chromophores.

Schematic representations of the energy levels and kinetic processes that are implied by the population state model are shown in Figure 9, parts A and B, respectively. The vertical arrows in Figure 9B represent the sum of three spin-allowed S_0/S_1 processes, i.e., absorption, fluorescence, and internal conversion. For states with more than one singlet exciton per molecule the vertical arrows include an additional process, singlet–singlet annihilation. The downward oriented diagonal arrows signify $S_1 \rightarrow T_1$ intersystem crossing. Reverse intersystem crossing is represented by the horizontal arrows. Finally, the upward oriented diagonal arrows signify triplet–triplet annihilation. The kinetic scheme represented in Figure 9B corresponds to a set of quasi-first-order processes with unequal rate constants. This implies an autocorrelation curve with a multiexponential decay. It should be noted, however, that based on estimates from data on bulk conjugated polymers it can be argued that the rate constants for the different processes in Figure 9B fall into a set of fast processes (singlet–singlet annihilation, intersystem crossing, internal conversion, emission of fluorescence, triplet–triplet annihilation) and a set of relatively slow processes (reverse intersystem crossing and formation of triplet excitons by $S_0 \rightarrow S_1$ excitation followed by intersystem crossing at low to moderate excitation rate).

B. Steady-State Solution for the Kinetic Scheme. Taking advantage of the large difference in rates for the fast vs slow processes we have applied the steady-state kinetic approximation for the appropriate states in Figure 9B, e.g. (2,0), (0,2), (3,0), (1,2), This analysis leads to an extremely simple and robust two-state model for conjugated polymers with a single exponentially decaying $G(\tau) = Ce^{-k\tau}$ and a set of relatively simple equations for the relevant physical processes (eqs 11–16). Due to the separation of time scales of the fast and slow processes, the conjugated polymer is predicted to spend most of its time in either (0,0) or (0,1) states, and correspondingly, only a small number of kinetic processes are significant. These processes are emphasized in Figure 9B by the bold arrows. Thus, the kinetic scheme reduces to an approximate two-state model,



where

$$k_F = k_{\text{exc}}k_{\text{isc}}\tau_{\text{fl}} \quad (12)$$

$$k_B = k'_{\text{isc}} + k_{\text{exc}}k_{\text{isc}}\tau'_{\text{fl}} \quad (13)$$

$$k = k_F + k_B \quad (14)$$

$$C = k_F k_B \left(\frac{1-f}{k_F f + k_B} \right)^2 \quad (15)$$

$$f = \frac{F_1}{F_0} = \frac{\tau'_{\text{fl}}}{\tau_{\text{fl}}} \quad (16)$$

Here all the parameters are analogous to those in eqs 2–5 except for τ'_{fl} , which is the fluorescence lifetime of the (1,1) state. Note that τ'_{fl} can be significantly shorter than τ_{fl} (the lifetime of (1,0)) due to an additional relaxation process for (1,1), namely singlet quenching induced by a triplet exciton. F_1/F_0 is the ratio of quantum yields (and instantaneous intensities) of the (1,1) and (1,0) states. Singlet quenching induced by a triplet exciton occurs via a Forster energy transfer process. The Forster energy transfer rate k_{ST} was estimated by using the MEH-PPV emission spectrum of an ensemble of single molecules and the transient absorption spectrum of MEH-PPV triplets⁶⁸ as a basis, and an orientation factor of 1. This calculation yields a k_{ST} of 10^{10} s^{-1} . The calculated value of k_{ST} corresponds within an order of magnitude with the values for k_{QST} (eqs 18 and 19) reported in Table 1.

V. Comparison to Experiment

Figure 10 demonstrates that the experimental data for C and k are highly consistent with “best-fit” predictions of the two-state theoretical model for representative molecules of MEH-PPV and F8BT. The experimental values are represented by black lines connecting the experimental C and k points which were determined by fitting the experimental $G(\tau)$ data by eq 6. The two-state kinetic model was fit to the experimental C and k values with a nonlinear least-squares procedure. The best-fit curves are plotted along with the experimental data in the upper two panels of Figure 10. In the fitting procedure τ_{fl} was fixed at the previously experimentally determined values, i.e., for F8BT $\tau_{\text{fl}} \sim 3 \times 10^{-9} \text{ s}$ and for MEH-PPV $\tau_{\text{fl}} \sim 200 \times 10^{-12} \text{ s}$.⁶⁹ The fitting parameters for representative MEH-PPV and F8BT molecules are shown in Table 1. The errors associated with the fitting process are indicated by significant numbers in Table 1. These data demonstrate the broad distribution of single molecule photophysical parameters observed in this study. We have not however investigated the distribution in detail for either compound.

The theoretical model is well able to account for the very different observed C vs I_E behavior for MEH-PPV and F8BT. In particular, MEH-PPV exhibits a strong dependence of C vs I_E over the entire excitation range (Figure 10), while for F8BT C is independent of I_E over a large range (Figures 8 and 10). The origin of this behavior is discussed in detail in the following sections of the paper, which are concerned with F8BT and MEH-PPV, respectively.

A. Excitation Intensity Dependence of C and k for F8BT.

A key prediction of eqs 12–16 that differs from the single chromophore case is the absence of a dependence of C on I_E for high I_E values, where annihilation is the dominant decay route for (0,1). This interesting and unprecedented physical effect (which is confirmed by experiment, see Figures 8 and 10, upper right panel) is a simple consequence of the fact that at high I_E both the forward (0,0) \rightarrow (0,1) and the reverse

TABLE 1: Best-Fit Kinetic Parameters for Typical MEH-PPV and F8BT Single Molecules^a

molecule	f	σ (cm ²)	k'_{isc} (s ⁻¹)	k_{QST} (s ⁻¹)
MEH-PPV	0.30	1.7×10^{-16}	6.0×10^3	7.8×10^9
MEH-PPV	0.03	2.5×10^{-16}	6.4×10^3	1.1×10^{11}
MEH-PPV	0.01	8.3×10^{-17}	3.8×10^3	3.4×10^{11}
MEH-PPV	0.22	2.9×10^{-16}	4.0×10^3	1.2×10^{10}
F8BT	0.36	8.1×10^{-16}	1.5×10^3	5.9×10^8

^a In the fitting procedures a quantum yield of intersystem crossing of 1.25% was used for MEHPPV,⁷³ and 2% for F8BT.

processes (0,1) \rightarrow (0,0) are linearly proportional to the rate of generation of triplets ($k_{exc}k_{isc}\tau_{fl}$).

To examine this point in more depth it is useful to quantitatively consider the dependence k vs I_E as shown in Figure 11A, which is predicted by eqs 12–14 to be linear. The zero intensity intercept (2.03 ± 0.05 ms⁻¹) is assigned based on eq 13 to k'_{isc} , the rate of reverse intersystem crossing for (0,1). The forward rate of intersystem crossing k_{isc} can be estimated from the slope of the k vs I_E line, using the measured absorption cross-section of F8BT (10^{-14} cm²) and fluorescence lifetime, τ_{fl} ($\sim 3 \times 10^{-9}$ s for F8BT). Using this method we obtain an estimate for k_{isc} of 6.7×10^6 s⁻¹. This ISC rate corresponds to a 2% quantum yield for the intersystem crossing, which is a typical value for conjugated polymers.

A key result is that at high power $k'_{isc} \ll k_{exc}k_{isc}\tau'_{fl}$, i.e., the reverse intersystem crossing rate is much smaller than the rate of triplet–triplet annihilation, so the latter process is dominant. This is demonstrated in the bottom panel of Figure 11, where experimentally determined values for k_F and k_B for the molecule in Figure 8 are shown. (These were calculated from eqs 12–16, using the experimentally determined C and k values, $k_{isc} = 6.7 \times 10^6$ s⁻¹ and $\tau_{fl} = 3 \times 10^{-9}$ s, see above.) In fact, for the reverse process in this excitation intensity range, two triplets are annihilated for every triplet that is generated, hence triplet generation is responsible for the rapid triplet decay. In this high-intensity regime (which we estimate to be at $I_E > 150$ W/cm² for F8BT), the contrast C can be approximated by the following relationship

$$C = \frac{1}{f} \left(\frac{1-f}{2} \right)^2 \quad (17)$$

which allows for a straightforward experimental determination of f from C . Furthermore, by using the known τ_{fl} and the relationship

$$1/\tau'_{fl} = 1/\tau_{fl} + k_{QST} \quad (18)$$

eqs 15–17 can be used to determine the effective first-order quenching rate constant of singlet excitons by triplet excitons in the same polymer chain (eq 19).

$$(1,1) \xrightarrow{k_{QST}} (0,1) \quad (19)$$

For the molecule in Figure 8, this corresponds to $k_{QST} = 5.9 \times 10^8$ s⁻¹. However, different molecules in the ensemble exhibit different C values as shown in Figure 7, which implies a distribution of k_{QST} values.

A different regime exists at very low excitation powers, where $k'_{isc} \gg k_{exc}k_{isc}\tau'_{fl}$, in which eqn 15 can be approximated by,

$$C = k_{exc}k_{isc}(1-f)/f \quad (20)$$

In this power range C is predicted according to eq 14 to decrease and become zero at the limit of zero excitation power. It is in

fact difficult to study the F8BT molecules in this regime ($I_E \ll 30$ W/cm²) due to background dark noise, which complicates the interpretation of C for low signal levels. Despite the very low excitation intensities used for the graph in Figure 8 relative to those usually used in SMS only one point in Figure 8 is actually in the low power regime.

Another important aspect of the SMS of conjugated polymers is the dependence of the steady-state fluorescence intensity F_{SS} on the excitation intensity, I_E , as shown in Figure 12 for F8BT. In contrast to the behavior of single chromophoric molecules the conjugated polymer does not show a significant saturation of the fluorescence intensity due to a buildup of triplet populations. This effect is easily explained by the steady-state model (eqs 12–16). According to this model, F_{SS} is given as follows:

$$F_{SS} = (1 - N_T)k_{exc}k_{rad}\tau_{fl} + N_Tk_{exc}k_{rad}\tau'_{fl} \quad (21)$$

Here k_{rad} is the radiative rate of singlet excitons and N_T is the number of triplet excitons per polymer chain.

$$N_T = \frac{k_{exc}k_{isc}\tau_{fl}}{(k_{exc}k_{isc}\tau_{fl} + k'_{isc} + k_{exc}k_{isc}\tau'_{fl})} \quad (22)$$

Equation 21 gives a linear “low excitation intensity” regime as follows,

$$F_{SS} \approx k_{rad}\tau_{fl} \left(\frac{I_E\sigma}{h\nu} \right) \quad (23)$$

in analogy with the single chromophore case. However, instead of saturation at high intensity a second linear regime “at high excitation intensity” is predicted, i.e.

$$F_{SS} \approx k_{rad}\tau_{fl} \left(\frac{I_E\sigma}{h\nu} \right) \{ (1 - N_{T,HI}) + N_{T,HI}f \} \quad (24)$$

where $N_{T,HI}$ is the number of triplets per polymer chain at high excitation intensity, i.e., $N_T = \tau_{fl}/(\tau_{fl} + \tau'_{fl})$.

Figure 10 shows that a linear regime at high excitation power is indeed consistent with predictions of the full two-state model for F8BT (see bottom panel, right-hand side). It should be emphasized that the linear regime implied by eq 24 is only valid in conditions where the steady-state approximation itself is valid. At sufficiently high excitation intensities it should be possible to excite the polymer chain sufficiently rapidly that annihilation should no longer be able to “keep up” with the generation of triplets and on average even more than one triplet per chain should be achievable, producing in principle saturation. However, over the range of excitation intensities in this study the predictions of eq 24 are in good agreement with the experiments and saturation is not observed for F8BT.

B. Correlation Results for MEH-PPV and the Role of Hole Polarons. Typical autocorrelation curves for a MEH-PPV single molecule as a function of excitation power are shown in Figure 13. As in the case of F8BT the $G(\tau)$ for MEH-PPV is well-fit by a single-exponential decay, with a relaxation rate that increases with excitation intensity I_E (Figure 13B). The C vs I_E dependence for MEH-PPV molecules reveals that higher excitation intensities are required for MEH-PPV compared to F8BT to enter the regime where C vs I_E is constant (Figure 10). For MEH-PPV, the F_{SS} vs I_E dependence shows curvature due to the transition from the low to high power linear regimes. A theoretical prediction of this effect is demonstrated for MEH-PPV in the bottom panel of the left-hand side of Figure 10.

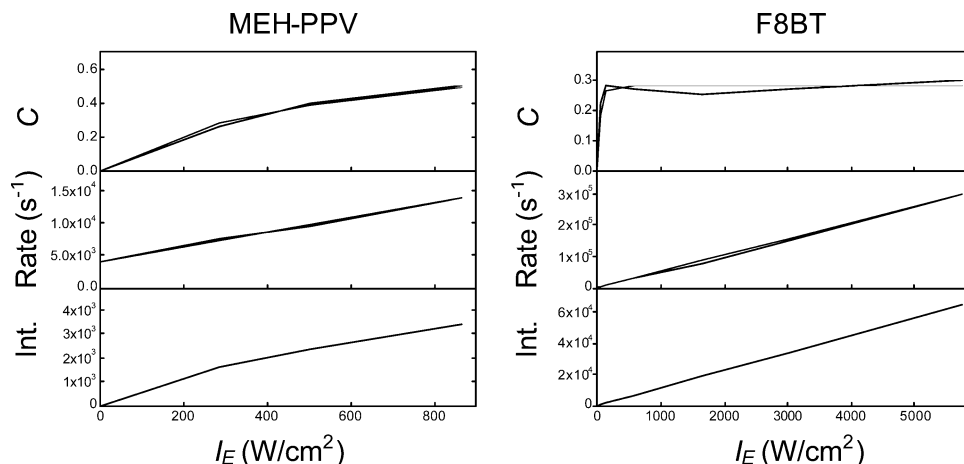


Figure 10. Experimental (black) and theoretical (gray) C and k values (top and middle panels, respectively) for MEH-PPV and F8BT (see text for further details). The bottom panels portray theoretical predictions for the mean value of $F(t)$ as a function of incident excitation intensity using the best-fit parameters from the data in the upper two panels. These plots show that the fluorescence intensity is not expected to saturate for MEH-PPV and F8BT in these experiments.

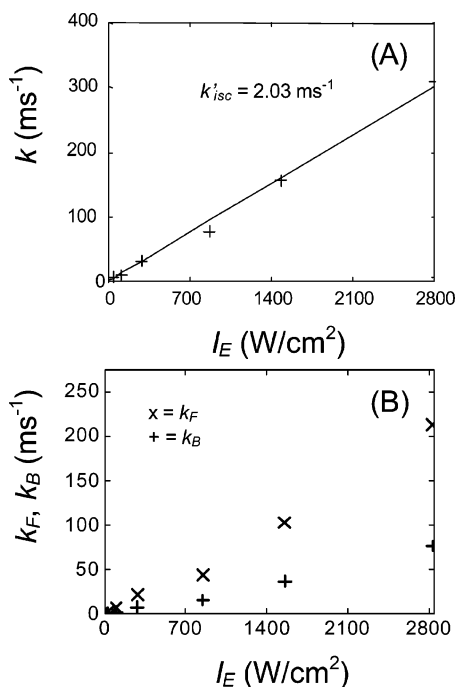
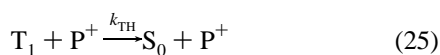


Figure 11. (A) Relaxation rate measured for a single F8BT molecule, plotted as a function of excitation intensity (also see Figure 8). The intercept at zero excitation intensity corresponds to k'_{isc} and is $2.03 \pm 0.05 \text{ ms}^{-1}$. (B) Calculated forward (k_F) (indicated by \times) and backward rate (k_B) (indicated by $+$) plotted as a function of excitation intensity. Both rates increase linearly with excitation intensity.

We have combined autocorrelation analysis with the recently introduced technique fluorescence-Voltage Single Molecule Spectroscopy (F-V/SMS)⁴¹ in order to investigate triplet quenching by hole polarons (P^+),



where k_{TH} is the bimolecular rate constant for triplet quenching by holes, and $k_{TH}[Q]$ is the pseudo-first-order quenching rate constant for a specific (voltage dependent) concentration. Figure 14 shows typical F-V/SMS data for MEH-PPV and a diagram of the F-V/SMS (capacitor-like) device that was used in the experiments. In F-V/SMS experiments, SMS data are acquired while simultaneously subjecting the molecules under investiga-

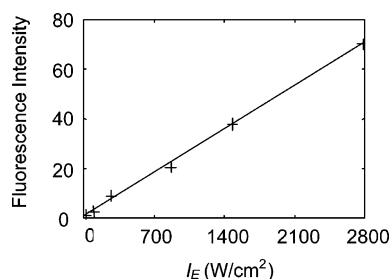


Figure 12. Plot of fluorescence intensity vs excitation intensity for a single F8BT molecule. The fluorescence intensity does not saturate under the experimental conditions employed in the experiments.

tion to a device-like environment with a periodically modulated electrical bias. A detailed discussion of this technique can be found elsewhere.⁴¹ For sufficiently positive biases the metal/hole transport layer (Au/TPD) functions as an “ohmic contact” and TPD holes are injected into the device. Under these conditions the device rapidly reaches equilibrium such that holes build up at the TPD/insulator (TPD/PMMA) interface. Since MEH-PPV is also located at the TPD/PMMA interface MEH-PPV is subject to collisions with TPD holes at positive bias. In contrast, at negative bias holes are removed from the device and MEH-PPV/TPD-hole collisions are no longer a factor. Figure 14B shows F-V/SMS data for a typical MEH-PPV molecule that is in contact with the TPD layer. Here the steady-state fluorescence intensity is plotted as a function of bias on the device. The actual $F(t)$ were acquired for ~ 100 – 150 cycles of the bias and the $F(t)$ data were synchronously averaged.

For negative bias the hole concentration is negligible and quenching of singlet and triplet excitons by holes is not a factor. Thus, in the negative bias region the fluorescence intensity is not a function of bias. Furthermore, the intensity autocorrelation data for negative bias (Figure 15A) is indistinguishable from that of MEH-PPV isolated in pure PMMA (e.g. Figures 3 and 13). A very different behavior is observed for the F-V/SMS data and the $G(\tau)$ curve near the threshold voltage region, i.e., where hole injection begins to be significant. At the threshold voltage, the steady-state fluorescence intensity shows no significant change relative to zero bias; however, $G(\tau)$ has no detectable transient. We assign this unprecedented effect to rapid triplet quenching by hole polarons, eq 25,

$$k_B = k'_{isc} + k_{exc}k_{isc}\tau'_{fl} + k_{TH}[Q] \quad (26)$$

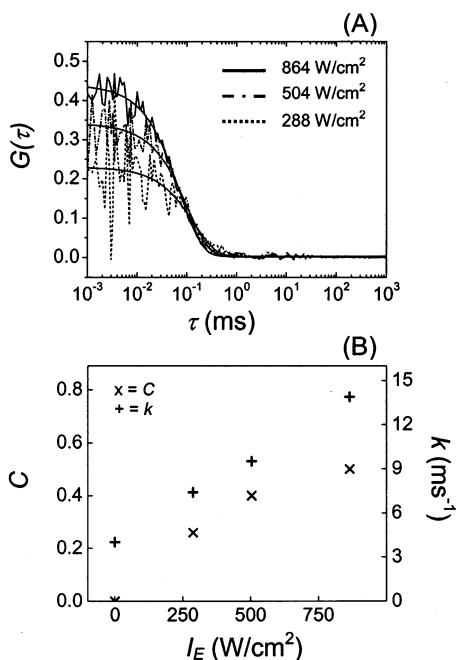


Figure 13. (A) Correlation data acquired for a single MEH-PPV molecule at different excitation intensities (i.e., 288, 504, and 864 W/cm^2) plotted along with best-fit single exponential decays. The smooth lines are single-exponential fits to the data. (B) Best-fit values for the relaxation rate k and autocorrelation amplitude C are indicated by + and \times , respectively. Both parameters increase linearly with excitation intensity.

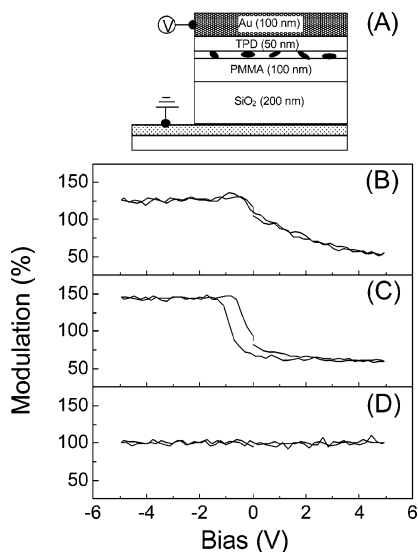


Figure 14. (A) Schematic representation of the capacitor-like device used for F-V/SMS and correlation experiments in which a bias is applied to the sample (see Figure 15). F-V/SMS data are shown for MEH-PPV molecules in oxygen-depleted devices (B), oxygen-rich devices (C), and an MEH-PPV molecule that is disconnected from the TPD hole transporting layer (D). The data in parts B and C represent diffusion-controlled quenching by hole polarons in the TPD layer and reversible hole injection in an MEH-PPV/OH⁻ complex, respectively.

which would have the effect of a significantly increased k_B , since a rapid $k_{\text{TH}}[Q]$ is predicted to have two consequences. First, the steady-state concentration of triplet excitons is predicted to decrease (k_F/k_B), allowing the steady-state fluorescence intensity to increase (as observed). Second, a sufficiently rapid k_B (i.e. triplet exciton decay $\gg 10^6 \text{ s}^{-1}$) would be characterized by a small amplitude $G(\tau)$, which is again consistent with experiment. Interestingly, at even higher biases

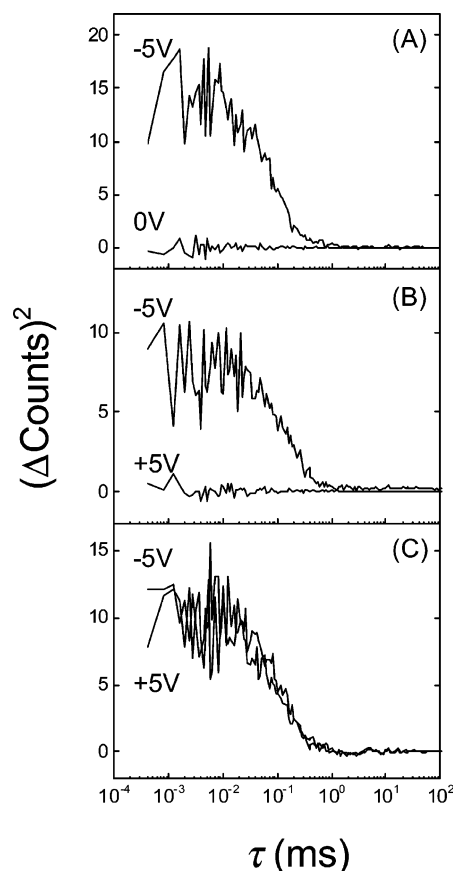


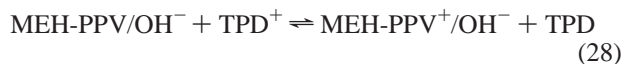
Figure 15. Autocorrelation data (not normalized by the total intensity) for individual molecules in a device such as shown in Figure 14A. The applied bias is indicated in the figure. The data in parts A–C correspond to molecules of the types shown in Figure 14B–D i.e., (A) efficient quenching of MEH-PPV triplets by hole polarons in the TPD layer (oxygen depleted device), (B) efficient quenching of MEH-PPV triplets by hole injection on the polymer chain (oxygen rich device), and (C) no effect of the applied bias on the MEH-PPV triplet population, since the molecule is electrically disconnected from the TPD layer. The latter observation shows that these phenomena are related to polarons in the device, not to an electrical field effect.

the fluorescence intensity actually decreases with increasing bias (as previously reported).^{41,42} In this bias range the triplet concentration is already very small due to a rapid $k_{\text{TH}}[Q]$ but an additional process, singlet quenching by hole polarons, i.e.



becomes a factor. This quenching process can occur either via energy transfer from the singlet exciton to the holes or via exciton dissociation induced by the holes which could be possible under the electrical fields we are using in the experiments.^{70–72} Note that these data imply that triplet quenching by holes is observed to be much more efficient than singlet quenching by holes, which is not surprising considering their relative lifetimes. Triplets have a lifetime on the order of tens to hundreds of microseconds depending on the annihilation rate for the I_E used in these studies, while singlets have a subnanosecond lifetime. An extreme example of singlet quenching by hole polarons is shown in Figure 14C (and analogously $G(\tau)$ in Figure 15B), which exhibits a sigmoidal F-V/SMS curve. For molecules of this type (which have been extensively discussed elsewhere)^{41,42} photooxidation with oxygen impurities alters the MEH-PPV HOMO energy, which allows S_0 to become oxidized at positive bias. In particular, it has been argued that photooxi-

dation produces a MEH-PPV molecule with hydroxide partner,



where TPD and TPD⁺ represent the neutral and charged form (hole) of TPD. For molecules of the type shown in the left-hand side of eq 28 the $G(\tau)$ data resemble those of isolated MEH-PPV with a triplet lifetime on the tens of microseconds scale, while at positive bias the $G(\tau)$ data reflect efficient triplet quenching by hole polarons, which in this case is presumably a MEH-PPV rather than TPD hole. Presumably, the small expected increase in fluorescence intensity at the threshold voltage due to triplet quenching and reduced quenching of singlets by triplets is masked by the very large signal due to singlet quenching from MEH-PPV S₀ oxidation. The latter process is essentially a single charge-transfer process that occurs over a much smaller bias range than that observed for molecules of the first type (i.e. Figures 14B and 15A). The third type of MEH-PPV molecules (Figures 14D and 15C) exhibit essentially no effect of bias and in fact resemble isolated MEH-PPV molecules that are apparently in poor contact with the TPD hole transporting layer. The absence of triplet and singlet quenching as a function of applied bias for molecules of the third type seems to confirm that the bias effects on the F-V/SMS data and $G(\tau)$ data are in fact due to hole polarons rather than simply an electric field effect.

VI. Conclusions and Summary

Single molecule autocorrelation spectroscopy has been used to study triplet exciton dynamics in isolated conjugated polymer molecules and independently in conjugated polymer nanoparticles in contact with a hole transport layer in a multilayer capacitor-like device.

For isolated molecules highly efficient triplet–triplet annihilation is observed on a broad range of excitation intensities. The experimental data are well modeled by an approximate two-state model. The model predicts that the contrast in the autocorrelation data is independent of excitation power at high excitation intensities, which corresponds well with the experimental observations for F8BT. In the case of MEH-PPV larger excitation intensities are required to enter this regime, due to the fact that this is a much larger system than F8BT.

Autocorrelation experiments were also performed on polymer molecules in a capacitor-like device. The polymer triplets are efficiently quenched by hole polarons, and this quenching is observed to be more efficient than hole polaron quenching of singlet excitons, due to the much longer lifetime of triplet excitons.

Acknowledgment. We greatly acknowledge support of this research by the NSF and the Robert A. Welch Foundation.

References and Notes

- (1) Kohle, A.; Wilson, J. S.; Friend, R. H. *Adv. Mater.* **2002**, *14*, 701.
- (2) Baldo, M. A.; O'Brien, D. F.; Thompson, M. E.; Forrest, S. R. *Phys. Rev. B* **1999**, *60*, 14422.
- (3) Barzda, V.; Vengris, M.; Valkunas, L.; Grondelle, R. v.; Amerongen, H. v. *Biochemistry* **2000**, *39*, 10468.
- (4) Hofkens, J.; Schroeyers, W.; Loos, D.; Cotlet, M.; Kohn, F.; Vosch, T.; Maus, M.; Herrmann, A.; Mullen, K.; Gensch, T.; De Schryver, F. C. *Spectrochim. Acta, Part A* **2001**, *57*, 2093.
- (5) Tinnefeld, P.; Buschmann, V.; Weston, K. D.; Sauer, M. *J. Phys. Chem. A* **2003**, *107*, 323.
- (6) Hofkens, J.; Cotlet, M.; Vosch, T.; Tinnefeld, P.; Weston, K. D.; Ego, C.; Grimsdale, A.; Mullen, K.; Beljonne, D.; Bredas, J. L.; Jordens,

- S.; Schweitzer, G.; Sauer, M.; De Schryver, F. *Proc. Natl. Acad. Sci. U.S.A.* **2003**, *100*, 13146.
- (7) Woo, H. S.; Graham, S. C.; Halliday, D. A.; Bradley, D. D. C.; Friend, R. H.; Burn, P. L.; Holmes, A. B. *Phys. Rev. B* **1992**, *46*, 7379.
- (8) Miranda, P. B.; Moses, D.; Heeger, A. J. *Phys. Rev. B* **2004**, *70*, 085212.
- (9) Wohlgenannt, M.; Jiang, X. M.; Vardeny, Z. V. *Phys. Rev. B* **2004**, *69*, 241204.
- (10) Rothe, C.; Monkman, A. P. *Phys. Rev. B* **2003**, *68*, 075208.
- (11) List, E. J. W.; Scherf, U.; Mullen, K.; Graupner, W.; Kim, C. H.; Shinar, J. *Phys. Rev. B* **2002**, *66*, 235203.
- (12) Zerza, G.; Rothler, B.; Sariciftci, N. S.; Gomez, R.; Segura, J. L.; Martin, N. J. *Phys. Chem. B* **2001**, *105*, 4099.
- (13) Stevens, M. A.; Silva, C.; Russell, D. M.; Friend, R. H. *Phys. Rev. B* **2001**, *63*, 165213.
- (14) Silva, C.; Stevens, M. A.; Russell, D. M.; Setayesh, S.; Mullen, K.; Friend, R. H. *Synth. Met.* **2001**, *116*, 9.
- (15) Herz, L. M.; Silva, C.; Phillips, R. T.; Setayesh, S.; Mullen, K. *Chem. Phys. Lett.* **2001**, *347*, 318.
- (16) Yip, W.-T.; Hu, D.; Yu, J.; Vanden Bout, D. A.; Barbara, P. F. *J. Phys. Chem. A* **1998**, *102*, 7564.
- (17) Kulzer, F.; Orrit, M. *Annu. Rev. Phys. Chem.* **2004**, *55*, 585.
- (18) Tamarat, P.; Maali, A.; Lounis, B.; Orrit, M. *J. Phys. Chem. A* **2000**, *104*, 1.
- (19) Moerner, W. E.; Orrit, M. *Science* **1999**, *283*, 1670.
- (20) Kumbhakar, M.; Nath, S.; Mukherjee, T.; Mittal, J. P.; Pal, H. J. *Photochem. Photobiol. C: Photochem. Rev.* **2004**, *5*, 113.
- (21) Ambrose, W. P.; Goodwin, P. M.; Jett, J. H.; Van Orden, A.; Werner, J. H.; Keller, R. A. *Chem. Rev.* **1999**, *99*, 2929.
- (22) Nie, S.; Zare, R. *Annu. Rev. Biophys. Biomol. Struct.* **1997**, *26*, 567.
- (23) Xie, X. S.; Trautman, J. K. *Annu. Rev. Phys. Chem.* **1998**, *49*, 441.
- (24) Summers, M. A.; Robinson, M. R.; Bazan, G. C.; Buratto, S. K. *Chem. Phys. Lett.* **2002**, *364*, 542.
- (25) Deniz, A. A.; Dahan, M.; Grunwell, J. R.; Ha, T. J.; Faulhaber, A. E.; Chemla, D. S.; Weiss, S.; Schultz, P. G. *Proc. Natl. Acad. Sci. U.S.A.* **1999**, *96*, 3670.
- (26) Kim, H. D.; Nienhaus, G. U.; Ha, T.; Orr, J. W.; Williamson, J. R.; Chu, S. *Proc. Natl. Acad. Sci.* **2002**, *99*, 4284.
- (27) Mehta, A. D.; Rief, M.; Spudich, J. A.; Smith, D. A.; Simmons, R. M. *Science* **1999**, *283*, 1689.
- (28) Talaga, D. S.; Lau, W. L.; Roder, H.; Tang, J.; Jia, Y.; DeGrado, W. F.; Hochstrasser, R. M. *Proc. Natl. Acad. Sci. U.S.A.* **2000**, *97*, 13021.
- (29) Zhuang, X.; Ha, T.; Kim, H. D.; Centner, T.; Labeit, S.; Chu, S. *Proc. Natl. Acad. Sci.* **2000**, *97*, 14241.
- (30) Cotlet, M.; Masuo, S.; Luo, G. B.; Hofkens, J.; Van der Auweraer, M.; Verhoeven, J.; Mullen, K.; Xie, X. L. S.; De Schryver, F. *Proc. Natl. Acad. Sci. U.S.A.* **2004**, *101*, 14343.
- (31) Haase, M.; Hubner, C. G.; Reuther, E.; Herrmann, A.; Mullen, K.; Basche, T. *J. Phys. Chem. B* **2004**, *108*, 10445.
- (32) Lippitz, M.; Hubner, C. G.; Christ, T.; Eichner, H.; Bordat, P.; Herrmann, A.; Mullen, K.; Basche, T. *Phys. Rev. Lett.* **2004**, *92*, 103001.
- (33) Vallee, R. A. L.; Cotlett, M.; Van der Auweraer, M.; Hofkens, J.; Mullen, K.; De Schryver, F. C. *J. Am. Chem. Soc.* **2004**, *126*, 2296.
- (34) Vandenbout, D. A.; Yip, W. T.; Hu, D. H.; Fu, D. K.; Swager, T. M.; Barbara, P. F. *Science* **1997**, *277*, 1074.
- (35) Yu, Z. H.; Barbara, P. F. *J. Phys. Chem. B* **2004**, *108*, 11321.
- (36) Yu, J.; Hu, D. H.; Barbara, P. F. *Science* **2000**, *289*, 1327.
- (37) Hu, D. H.; Yu, J.; Wong, K.; Bagchi, B.; Rosicky, P. J.; Barbara, P. F. *Nature* **2000**, *405*, 1030.
- (38) Bartko, A. P.; Dickson, R. M. *J. Phys. Chem. B* **1999**, *103*, 3053.
- (39) Huser, T.; Yan, M.; Rothberg, L. J. *P. Natl. Acad. Sci. U.S.A.* **2000**, *97*, 11187.
- (40) Mehta, A.; Kumar, P.; Dadmun, M. D.; Zheng, J.; Dickson, R. M.; Thundat, T.; Sumpter, B. G.; Barnes, M. D. *Nano Lett.* **2003**, *3*, 603.
- (41) Gesquiere, A. J.; Park, S. J.; Barbara, P. F. *J. Phys. Chem. B* **2004**, *108*, 10301.
- (42) Park, S. J.; Gesquiere, A. J.; Yu, J.; Barbara, P. F. *J. Am. Chem. Soc.* **2004**, *126*, 4116.
- (43) Sartori, S. S.; De Feyter, S.; Hofkens, J.; Van der Auweraer, M.; De Schryver, F.; Brunner, K.; Hofstraat, J. W. *Macromolecules* **2003**, *36*, 500.
- (44) Muller, J. G.; Lemmer, U.; Raschke, G.; Anni, M.; Scherf, U.; Lupton, J. M.; Feldmann, J. *Phys. Rev. Lett.* **2003**, *91*, 267403.
- (45) Kumar, P.; Mehta, A.; Mahurin, S. M.; Dai, S.; Dadmun, M. D.; Sumpter, B. G.; Barnes, M. D. *Macromolecules* **2004**, *37*, 6132.
- (46) Hu, D. H.; Yu, J.; Barbara, P. F. *J. Am. Chem. Soc.* **1999**, *121*, 6936.
- (47) Lammi, R. K.; Fritz, K. P.; Scholes, G. D.; Barbara, P. F. *J. Phys. Chem. B* **2004**, *108*, 4593.
- (48) Ronne, C.; Tragardh, J.; Hessman, D.; Sundstrom, V. *Chem. Phys. Lett.* **2004**, *388*, 40.

- (49) Hollars, C. W.; Lane, S. M.; Huser, T. *Chem. Phys. Lett.* **2003**, *370*, 393.
- (50) Sun, W. Y.; Hsu, J. H.; Yang, S. C.; White, J. D.; Fann, W. S. *J. Lumin.* **2002**, *98*, 41.
- (51) Wang, C. F.; White, J. D.; Lim, T. L.; Hsu, J. H.; Yang, S. C.; Fann, W. S.; Peng, K. Y.; Chen, S. A. *Phys. Rev. B* **2003**, *67*, 035202.
- (52) Schindler, F.; Lupton, J. M.; Feldmann, J.; Scherf, U. *Proc. Natl. Acad. Sci. U.S.A.* **2004**, *101*, 14695.
- (53) Hubner, C. G.; Renn, A.; Renge, I.; Wild, U. P. *J. Chem. Phys.* **2001**, *115*, 9619.
- (54) English, D. S.; Furube, A.; Barbara, P. F. *Chem. Phys. Lett.* **2000**, *324*, 15.
- (55) Trautman, J. K.; Macklin, J. J. *Chem. Phys.* **1996**, *205*, 221.
- (56) Weston, K. D.; Carson, P. J.; DeAro, J. A.; Buratto, S. K. *Chem. Phys. Lett.* **1999**, *308*, 58.
- (57) Hu, D.; Yu, J.; Barbara, P. *J. Am. Chem. Soc.* **1999**, *121*, 6936.
- (58) Boiron, A. M.; Lounis, B.; Orrit, M. *J. Chem. Phys.* **1996**, *105*, 3969.
- (59) Tamarat, P.; Lounis, B.; Bernard, J.; Orrit, M.; Kummer, S.; Kettner, R.; Mais, S.; Basche, T. *Phys. Rev. Lett.* **1995**, *75*, 1514.
- (60) Lounis, B.; Moerner, W. E. *Nature* **2000**, *407*, 491.
- (61) Lounis, B.; Jelezko, F.; Orrit, M. *Phys. Rev. Lett.* **1997**, *78*, 3673.
- (62) Fleury, L.; Segura, J. M.; Zumofen, G.; Hecht, B.; Wild, U. P. *Phys. Rev. Lett.* **2000**, *84*, 1148.
- (63) Brunel, C.; Lounis, B.; Tamarat, P.; Orrit, M. *Phys. Rev. Lett.* **1998**, *81*, 2679.
- (64) Basche, T.; Moerner, W. E.; Orrit, M.; Talon, H. *Phys. Rev. Lett.* **1995**, *69*, 1516.
- (65) Note: At low excitation intensity the background intensity should be taken into account as follows: $C = (F_s / (F_s + F_b))^{2k_F/k_B}$, where F_s is the average detected fluorescence intensity and F_b is the average detected background intensity.
- (66) Note: For other systems at high excitation intensity this rate was accelerated, but this is not observed here.
- (67) English, D. S.; Harbron, E. J.; Barbara, P. F. *J. Phys. Chem. A* **2000**, *104*, 9057.
- (68) Monkman, A. P.; Burrows, H. D.; Miguel, M. D.; Hamblett, I.; Navaratnam, S. *Chem. Phys. Lett.* **1999**, *307*, 303.
- (69) Smilowitz, L.; Hays, A.; Heeger, A. J.; Wang, G.; Bowers, J. E. *Synth. Met.* **1993**, *55*, 249.
- (70) Gulbinas, V.; Zaushitsyn, Y.; Bassler, H.; Yartsev, A.; Sundstrom, V. *Phys. Rev. B* **2004**, *70*, 035215.
- (71) Gulbinas, V.; Zaushitsyn, Y.; Sundstrom, V.; Hertel, D.; Bassler, H.; Yartsev, A. *Phys. Rev. Lett.* **2002**, *89*, 107401.
- (72) Zaushitsyn, Y.; Gulbinas, V.; Zigmantas, D.; Zhang, F. L.; Inganas, O.; Sundstrom, V.; Yartsev, A. *Phys. Rev. B* **2004**, *70*, 075202.
- (73) Burrows, H. D.; de Melo, J. S.; Serpa, C.; Arnaut, L. G.; Miguel, M. D.; Monkman, A. P.; Hamblett, I.; Navaratnam, S. *Chem. Phys.* **2002**, *285*, 3.